Rab11 rescues synaptic dysfunction and behavioural deficits in a *Drosophila* model of Huntington's disease

Joern R. Steinert[1],[†], Susanna Campesan[2],[†], Paul Richards[1], Charalambos P. Kyriacou[2], Ian D. Forsythe[1] and Flaviano Giorgini[2],*

[1]MRC Toxicology Unit, University of Leicester, Hodgkin Building, Lancaster Road, Leicester LE1 9HN, UK
[2]Department of Genetics, University of Leicester, University Road, Leicester LE1 7RH, UK

Synapse abnormalities in Huntington's disease (HD) patients can precede clinical diagnosis and neuron loss by decades. The polyglutamine expansion in the huntingtin (htt) protein that underlies this disorder leads to perturbations in many cellular pathways, including the disruption of Rab11-dependent endosomal recycling. Impairment of the small GTPase Rab11 leads to the defective formation of vesicles in HD models and may thus contribute to the early stages of the synaptic dysfunction in this disorder. Here, we employ transgenic *Drosophila melanogaster* models of HD to investigate anomalies at the synapse and the role of Rab11 in this pathology. We find that the expression of mutant htt in the larval neuromuscular junction decreases the pre-synaptic vesicle size, reduces quantal amplitudes and evoked synaptic transmission and alters larval crawling behaviour. Furthermore, these indicators of early synaptic dysfunction are reversed by the overexpression of Rab11. This work highlights a potential novel HD therapeutic strategy for early intervention, prior to neuronal loss and clinical manifestation of disease.

INTRODUCTION

Neurodegenerative disorders such as Huntington's disease (HD), Alzheimer's disease and Parkinson's disease are devastating fatal conditions characterized by the death of specific populations of neurons. HD is an autosomal dominant disorder caused by the expansion of a polyglutamine tract in the huntingtin (htt) protein (1). Loss of medium spiny neurons in the striatal region of the brain is associated with many of the characteristic locomotor and cognitive deficits of HD (2). The underlying mechanisms contributing to this neuronal loss have been extensively explored and appear to be due to a myriad of cellular perturbations (3). These events may be critical for HD pathogenesis, but the neuronal and synaptic dysfunction occurs decades before the clinical onset of disease and probably contributes to early cognitive changes in patients (4–6).

Both clinical and mouse studies suggest that the synaptic dysfunction in HD comprises several related anomalies at the synapse, including, but not limited to, dendritic spine loss, reduced synaptic connectivity, glutamatergic signal transduction and presynaptic reduction of brain-derived neurotrophic factor (7). These changes may not only contribute to early abnormalities, but could also sensitize the relevant neurons to other pathological stresses, as well as normal aging processes. Importantly, the mechanistic dissection of synaptic disorder has therapeutic relevance, since synapses have the capacity for plasticity, growth and expansion, whereas the loss of neuronal cell bodies is difficult to reverse (8).

Recent studies have shown that the small Rab-family GTPase Rab11, which plays a key role in endosomal recycling (9–11), is functionally perturbed in several models of HD (12–15). Indeed, the inhibition of Rab11 activity by mutant htt impairs vesicle formation from recycling endosomes in HD patient fibroblasts (13). We recently found that Rab11 abrogated the loss of dendritic spines in primary murine neurons expressing mutant htt, suggesting that Rab11 may

---

*To whom correspondence should be addressed. Tel: +44 1162523485; Fax: +44 1162523378; Email: fg36@le.ac.uk
†Authors made equal contributions.
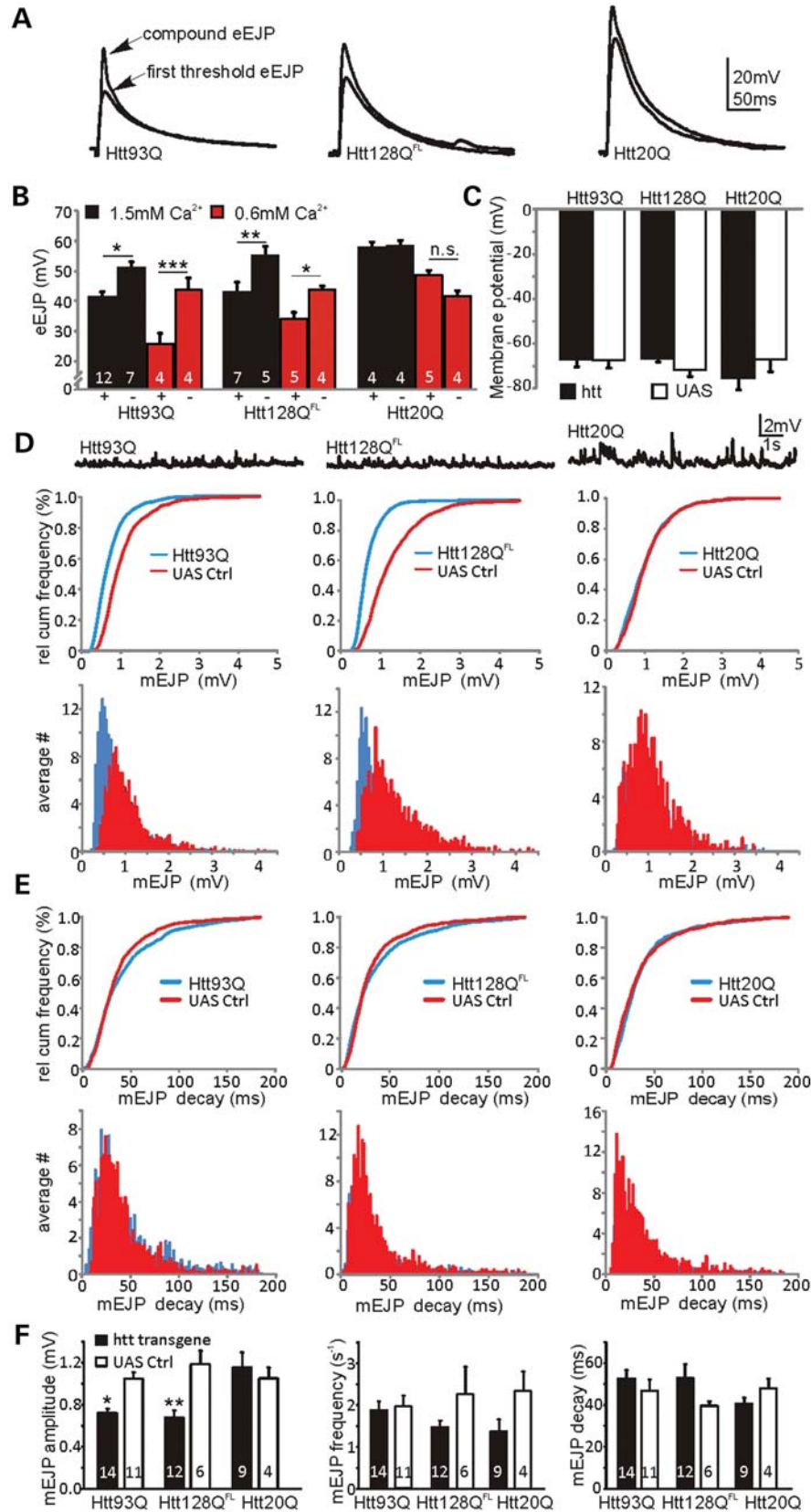
play a critical early role in the synaptic dysfunction observed in HD (15). Furthermore, Rab11 overexpression reduced neurodegeneration in a fruit fly model of HD and also extended lifespan and ameliorated defective emergence of the adult fly from the pupal case (15).

Here, we consolidate and extend these observations by exploring the role of Rab11 in the synaptic dysfunction at the *Drosophila* larva neuromuscular junction (NMJ), a well-established model of glutamatergic synaptic transmission (16). The larval NMJ is organized into presynaptic boutons rich in synaptic vesicles (SVs), active zones and a subsynaptic reticulum with the dense expression of glutamate receptors. Employing a multipronged approach, we find that mutant htt reduces the miniature excitatory junction potential (mEJP) amplitudes produced by the release of individual SVs (i.e. quantal size) at the NMJ and that this is likely due to smaller SV volume, subsequently leading to a reduction in evoked EJP (eEJP) amplitudes. Furthermore, we find that the restoration of SV size via Rab11 overexpression is sufficient to completely rescue quantal size. Finally, behavioural defects observed in larvae expressing mutant htt can also be abrogated by Rab11 overexpression. These results demonstrate that Rab11 plays an important role in the early synaptic dysfunction caused by mutant htt and that interventions targeting Rab11 function prior to the clinical manifestation of disease may have therapeutic relevance for HD.

RESULTS

Mutant htt-expressing larval NMJs show a reduced quantal size and evoked release

The fruit fly *Drosophila melanogaster* has been extensively exploited for the study of HD and other polyglutamine disorders (17). A robust and widely used model of HD has been generated using the UAS/Gal4 bipartite expression system to drive the pan-neuronal expression of a human exon 1 fragment of mutant htt (Htt93Q) with the *elav-GAL4* driver (18). These flies present several disease-relevant phenotypes, including neurodegeneration, shortened lifespan and locomotor deficits. An alternate model expressing full-length mutant htt has also been developed (Htt128Q^{FL}), which though less severe than the Htt93Q flies, also exhibits several phenotypes reminiscent of disease pathology (19).

In order to investigate early events in presynaptic dysfunction, we studied synaptic transmission at the NMJ of third instar larvae with the pan-neuronal expression of either Htt93Q or Htt128Q^{FL} under physiological conditions in a haemolymph-like buffer with 1.5 mM Ca^{2+} (HL-3). A previous study found a potentiation of transmitter release in Htt128Q^{FL}

larvae in lower HL-3 Ca^{2+} concentrations (a modest increase at 0.6 mM and a dramatic ~5-fold increase at 0.25 mM) (19). We thus also repeated recordings in lowered Ca^{2+} (0.6 mM) and found identical eEJP amplitude values in Htt128Q^{FL} larvae as Romero *et al.* (19) (Fig. 1A and B). However, these values represented a reduction in eEJP amplitudes in both Htt93Q and Htt128Q^{FL} larvae compared with their corresponding UAS controls when recorded at either 0.6 or 1.5 mM Ca^{2+} concentration. Larvae expressing a control Htt20Q exon 1 fragment did not show different eEJP amplitudes at either Ca^{2+} concentration [Fig. 1A and B, three-way analysis of variance (ANOVA), htt background $F_{2,52} = 16.6$, $P < 0.0001$; transgene expression $F_{1,52} = 19.05$, $P < 0.0001$, Ca^{2+} concentration $F_{1,52} = 50.7$, $P \sim 0$ and htt background × transgene expression interaction $F_{2,52} = 10.1$, $P < 0.0002$]. Furthermore, we did not observe significantly altered eEJP amplitudes in larvae with the *elav*-driven expression of a full-length htt control (Htt16Q^{FL}) or Gal4 alone at physiological Ca^{2+} concentrations (Supplementary Material, Fig. S1). The background × transgene interaction is reflected in the significant *post-hoc* pairwise differences between the expressed and the control genotypes among the different htt backgrounds (Fig. 1B). In order to compare uncorrected eEJP amplitudes, we observed that resting membrane potentials were similar between conditions at both Ca^{2+} doses (shown for 1.5 mM Ca^{2+} in Figure 1C, three-way ANOVA, no significant F-ratios), with mean potentials ranging between -67 ± 3 and -75 ± 5 mV. Thus, the effects of non-linear summation are likely to be small and amplitude correction was unnecessary.

Changes in eEJP amplitudes can be caused by altered quantal size (20,21), changes in release probability (22,23) or glutamate receptor composition/expression (24). In order to identify the underlying mechanisms for the observed eEJP amplitude changes in mutant htt-expressing larval NMJs, we analysed mEJPs in all three htt-expressing lines. As shown in Figure 1D, average relative cumulative frequency histograms and histograms for mEJP amplitudes demonstrated an increased probability of small amplitude events and hence a left shift in mEJP amplitude distributions in Htt93Q [Kolmogorov−Smirnov (K-S) test, $D = 0.38$, $P < 0.0001$] and Htt128Q^{FL} larvae ($D = 0.54$, $P < 0.0001$) compared with UAS controls, and no change in Htt20Q expressing larvae ($D = 0.087$, $P = 0.88$). Htt16Q^{FL} and Gal4 control larvae exhibited no change in mEJP amplitudes at physiological Ca^{2+} concentrations (Supplementary Material, Fig. S1). These data strongly indicate that mutant htt-mediated eEJP alterations are due to a reduced quantal amplitude or glutamate receptor dynamics.

The predominant *Drosophila* postsynaptic glutamate receptors are *D*GluRIIa and *D*GluRIIb, each of which has distinct decay kinetics (24) and which both compete for access to

Figure 1. Mutant htt expression causes a reduction in evoked transmission and quantal size. (**A**) Evoked (eEJP) recordings from *Drosophila* larvae NMJs expressing Htt93Q, Htt128Q^{FL} or Htt20Q constructs recorded in HL-3. Note, arrows indicate first threshold and compound peaks. (**B**) eEJP amplitudes are reduced in larvae expressing Htt93Q and Htt128Q^{FL} at both 1.5 mM (black) and 0.6 mM (red) extracellular Ca^{2+} (mean $\pm$ SEM with *n* indicated within each bar). Comparisons are between htt transgene expressing ($+$) and UAS control ($-$) larvae. Expression of Htt20Q has no effect on eEJPs. (**C**) Mean resting membrane potentials are similar between genotypes. (**D**) Top, sample mEJP recordings for the genotypes indicated. Middle, relative cumulative frequency histograms for the mEJP amplitudes (Htt93Q and Htt128Q^{FL} have different distributions versus controls, K-S test: $P < 0.0001$ in both cases, Htt20Q was not different from control). Bottom, mEJP amplitude histograms indicate the left shift of mEJPs in Htt93Q and Htt128Q^{FL} but not in Htt20Q. (**E**) Top, relative cumulative frequency histograms for the mEJP decay kinetics (Htt93Q, Htt128Q^{FL} and Htt20Q do not show significantly different distributions, K-S test: $P > 0.05$ in all cases). Bottom, mEJP decay kinetics histograms in Htt93Q, Htt128Q^{FL} and Htt20Q. (**F**) Summary graphs for mEJP amplitudes (left), frequencies (middle) and decay (right). ANOVA with *post hoc* tests (see Materials and methods). *$P < 0.05$, **$P < 0.01$ and ***$P < 0.001$.

*D*GluRIII (25) and subsequent localization to the synapse. As mEJP decay kinetics are similar between all genotypes (K-S test, $P > 0.05$ for each genotype; Fig. 1E), our data imply that postsynaptic *D*GluRs are not affected by mutant htt expression and consistent with a presynaptic mutant htt-induced malfunction. In agreement with previous results, we found mean mEJP amplitudes in all UAS and Htt20Q control larvae to be approximately 1 mV (21,24,26,27), while Htt128Q^{FL} expression gave significantly smaller mean mEJP amplitudes of ~0.7 mV (19), as did Htt93Q, confirming the suppression of quantal size relative to Htt20Q and UAS control larvae (Fig. 1F, two-way ANOVA, htt background × transgene expression interaction $F_{2,50} = 4.47$, $P = 0.016$). We also examined mEJP frequencies, which showed a marginally significant effect for transgene expression (two-way ANOVA, $F_{1,50} = 4.94$, $P = 0.03$), but *a posteriori* tests did not confirm this difference in any of the three htt backgrounds, and ANOVA did not reveal any significant effects for decay kinetics (Fig. 1F). As Htt93Q and Htt128Q^{FL} yielded similar effects on neurotransmission, we focused on the Htt93Q model of synaptic dysfunction in the experiments below.

Electrophysiological deficits are correlated with changes in SV size and are rescued by Rab11 overexpression

To investigate whether the observed decrease in mEJP amplitudes was caused by a reduction in SV size, we undertook ultra-structural analysis of NMJ boutons. The *Drosophila* NMJ possesses two types of boutons, with 1s boutons harbouring larger vesicles (~45 nm diameter) and 1b boutons containing smaller vesicles (~38 nm) (20). Resting synaptic activity appears to arise primarily by SV release from 1b boutons, as little activity is observed from 1s boutons, underscoring the different functionality of these synapses in terms of release. We have previously shown that the expression of a mutant htt exon 1 fragment causes defects in local endosomal recycling mediated by the Rab11 protein (15). Therefore, Rab11 could be involved in the observed mutant htt-induced reduction in quantal size by affecting SV size. To test this, we directly measured SV size using electron microscopy. The outer diameters of the SV were measured in both 1s and 1b boutons from UAS control (Fig. 2A–D) and Htt93Q larvae, as well as larvae overexpressing both Htt93Q and Rab11. Histograms and cumulative probability plots of the data showed a left-shifted distribution of vesicle sizes in Htt93Q larvae (i.e. larger relative number of smaller vesicles compared with control) with the average vesicle size significantly reduced (Fig. 2E–H). This shift and the average diameter were completely restored in both 1s and 1b boutons from Htt93Q larvae overexpressing Rab11 (Fig. 2E–H).

In addition to changes in SV size, we also observed that NMJ boutons expressing Htt93Q showed increased numbers of vacuoles (Supplementary Material, Fig. S2D and J), multi-lammelar bodies (Supplementary Material, Fig. S2E) and multivesicular bodies (Supplementary Material, Fig. S2B). These are all markers of increased lysosomal/autophagic pathways and demonstrate that the synapse has diverted membrane material into degradative pathways (28). Nevertheless, Htt93Q expression did not affect the number of active zones with SVs clustering around synaptic dense areas or T-bars,

which are indicative of active functional synapses (29) (Supplementary Material, Fig. S2M). Quantifying numbers of active zones per micrometre of membrane revealed no difference between any of the strains (Supplementary Material, Fig. S2M). We can conclude that active synaptic regions are preserved in third instar larvae expressing Htt93Q, further underscoring that the observed electrophysiological defects are consistent with a reduced SV size.

We postulated that the amelioration of SV size by Rab11-overexpression could directly affect the electrophysiological properties of mEJP and eEJP recordings in Htt93Q larvae. To test this, we compared both eEJPs and mEJPs in Htt93Q expressing larvae in the absence and the presence of the Rab11 overexpression transgene. We found that the overexpression of Rab11 rescues the mutant htt-induced reduction in eEJP amplitudes to levels comparable with control Rab11-expressing larvae ($F_{2,21} = 4.46$, $P = 0.024$, Fig. 3A and B), while mean resting membrane potentials were similar between groups (approximately -69 ± 5 mV, $F_{2,24} = 0.98$, n.s., Fig. 3C). The rescuing effect on eEJP amplitudes was due to larger mEJP amplitudes following Rab11 expression in Htt93Q larvae (Fig. 3D; $D = 0.25$, $P = 0.006$). Also, there was no significant difference observed in mEJP decay kinetics following Rab11 expression (Fig. 3E; $D = 0.053$, $P = 0.99$). Comparison of mean mEJP amplitudes (Fig. 3Fi) indicates that Rab11 overexpression completely rescued the electrophysiological deficits caused by Htt93Q expression ($F_{2,28} = 8.04$, $P < 0.002$), but no significant effects were observed for either mEJP frequency or decay kinetics (Fig. 3Fii and iii). When we compared the quantal content (i.e. the number of SV released during a synaptic event) among Htt93Q, Htt93Q/Rab11 and Rab11 overexpressing larvae, we found no significant difference (Fig. 3Fiv, $F_{2,16} = 2.84$, $P = 0.09$), suggesting that the reduced eEJP amplitudes in Htt93Q-overexpressing larvae are entirely due to the reduction in quantal size, further excluding potential effects on the presynaptic release machinery or post-synaptic *D*GluR-IIs (30).

To ensure that the protective effects of Rab11 overexpression were not due to the titration of Gal4-induced expression from the additional UAS transgene present in these larvae, we co-expressed Htt93Q with the control protein dsRED and observed no alteration in the mutant htt-induced electrophysiological deficits (Supplementary Material, Fig. S1). Together, these data show that Rab11 overexpression rescues the physiological deficit arising from the mutant htt-dependent reduction in quantal size and evoked transmitter release. This work also illustrates a novel interaction of mutant htt with SV formation, ultimately leading to synaptic dysfunction, which may contribute to HD pathogenesis.

Rab11 ameliorates locomotor activity deficits in mutant htt expressing larvae

Drosophila larvae exhibit stereotypical crawling behaviour when placed upon an agarose surface (31). Perturbations in crawling have been used to study flies with mutations in various ion channels, including mechanosensitive channels, as well as *Drosophila* models of neurodegeneration (32–35). Larval crawling is characterized by periods of movement in
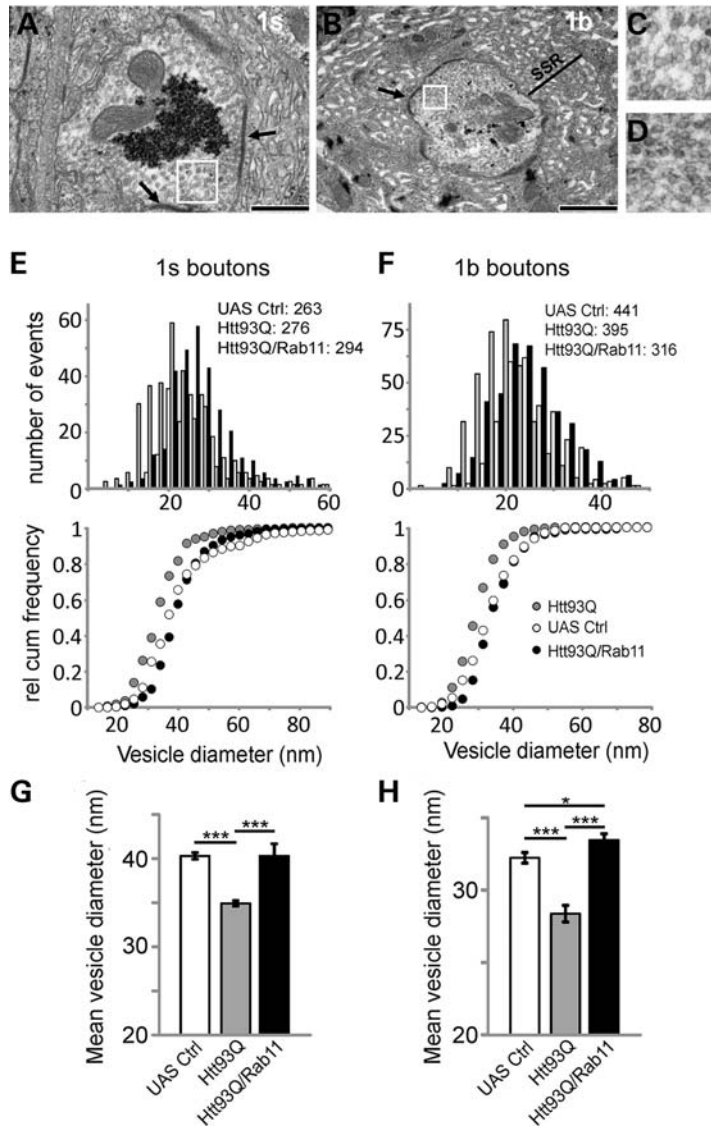
Figure 2. The reduced vesicle size in Htt93Q fruit fly larvae is fully restored by Rab11 overexpression. (**A**) EM image of a 1s synaptic bouton showing the synaptic active zone (arrows) and SVs (box) in UAS control larvae. Scale bar = 500 nm. (**B**) 1b bouton with active zones (arrow), SVs (box) and subsynaptic reticulum (SSR) in UAS control larvae. Scale bar = 1 μm. (**C**) The 2.5-fold magnification of SVs (box) from (A). (**D**) 5-fold magnification of SVs (box) from panel (B). Histogram and relative cumulative frequency plots of SV size for 1s (**E**) and 1b (**F**) boutons showing left shift (smaller vesicles) in Htt93Q larvae compared with UAS control (numbers indicate counted vesicles per genotype). Rab11 overexpression restores vesicle size. (**G** and **H**) The average vesicle size for both boutons and the condition indicated. The mean vesicle size in Htt93Q larvae is smaller compared with UAS control. Vesicle size is restored for both 1s and 1b boutons when Rab11 is expressed. ANOVA with *post hoc* tests $^{*}P < 0.05$ and $^{***}P < 0.0001$.

a particular direction interrupted by turns. Thus, traces made of larval crawling patterns allow the determination of several metrics describing crawling behaviour, such as distance travelled or number of turns performed during a defined period of time (21,31) (Fig. 4A and B).

Having already shown that Rab11 ameliorated SV and quantal size abnormalities, we postulated that Rab11 overexpression might further ameliorate any behavioural defects in Htt93Q larvae associated with altered quantal size. To address this question, we analysed crawling in larvae expressing Htt93Q, Htt20Q or Htt93Q/Rab11, as well as appropriate control larvae, in motor neurons using the *c164-GAL4* driver (36). Htt93Q larvae performed significantly fewer turns than

those expressing Htt20Q or control larvae ($F_{4,141} = 8.44$, $P \sim 0$, pairwise *a posteriori* values $P = 0.006$, $P \sim 0$, respectively, Fig. 4C). Htt93Q larvae also exhibited a correlated significant increase in distance travelled (Fig. 4D, $F_{4,151} = 11.7$, $P \sim 0$), suggesting that reducing the number of turns permits larvae to crawl further. Normalizing distance data by the number of turns (distance/turn) enhance the resolution of these behavioural abnormalities observed in Htt93Q larvae compared with Htt20Q larvae and other controls (Fig. 4E, $F_{4,151} = 7.9$, $P \sim 0$, pairwise *a posteriori* values $P = 0.0007$ to $P \sim 0$). Strikingly, Htt93Q larvae overexpressing Rab11 showed a complete rescue of the larval phenotype based on the numbers of turns, distance travelled or distance/
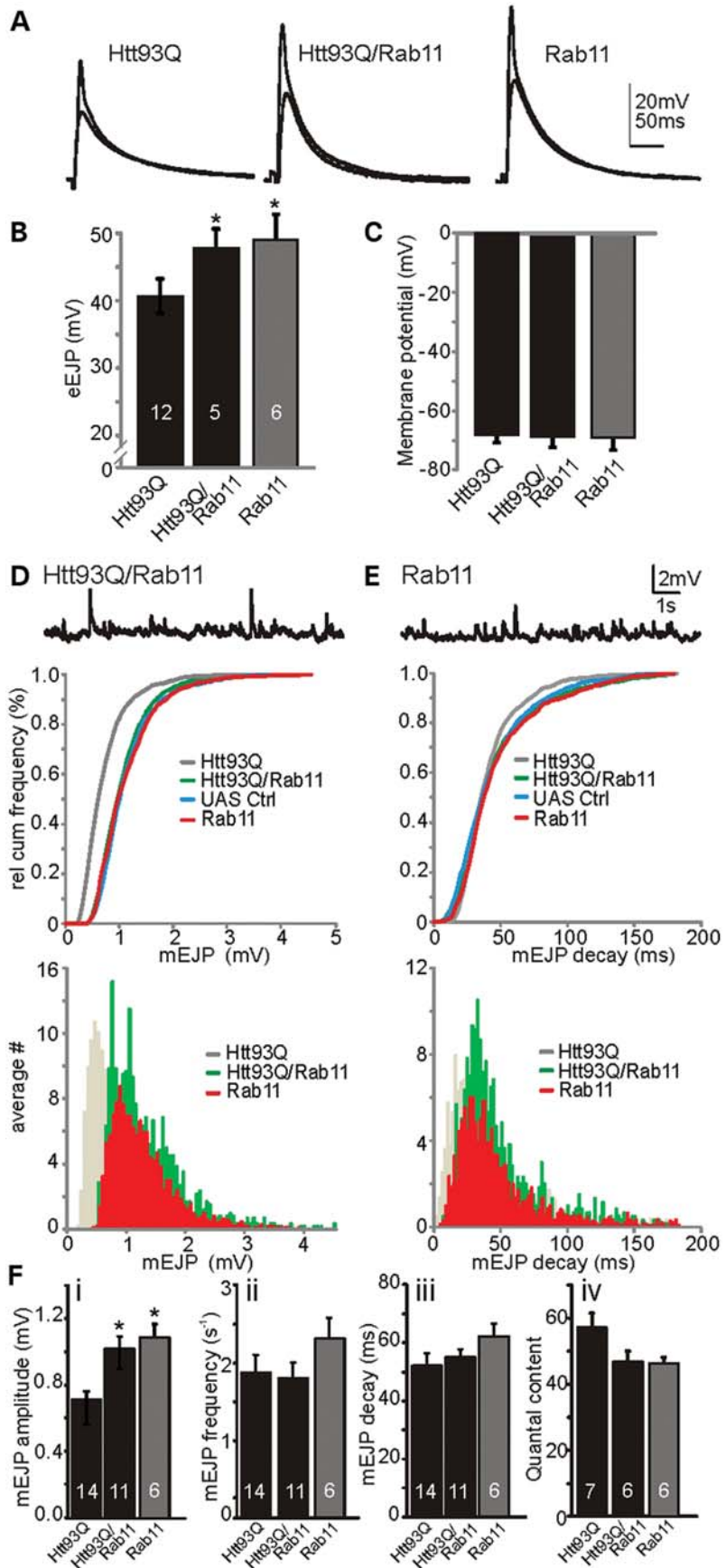
turn ($P = 0.0002$ to $P \sim 0$, respectively). These results complement our electrophysiological observations and indicate that the restoration of synaptic transmission by Rab11 overexpression recovers the disrupted behavioural readouts of larvae expressing mutant htt.

DISCUSSION

The majority of research on HD and other neurodegenerative disorders has focused on elucidating the mechanisms underlying neurodegeneration and identifying therapeutic interventions that prevent cell death. However, it is clear that the neuronal and synaptic dysfunction occurring prior to neuronal death plays an important role in the pathogenesis of the disease (7). Here, we find that mutant htt causes a synaptic dysfunction at the larval *Drosophila* NMJ by decreasing the SV size, and ultimately impairing synaptic transmission. Restoration of SV volume by the overexpression of Rab11 as shown by an electron microscopy is sufficient to completely restore synaptic function at the electrophysiological level, thereby implicating Rab11 in these processes. The observed synaptic deficits correlate with abnormal larval behaviour which was also ameliorated by Rab11 overexpression. These observations support a model in which mutant htt alters SV size, leading to synaptic and behavioural dysfunction that Rab11 overexpression is able to reverse (Fig. 5).

Our observations complement previous work in HD patient fibroblasts showing that mutant htt inhibits the activation of Rab11 (the guanosine triphosphate (GTP)-bound form) and that the disruption of this process leads to the defective formation of vesicles from recycling endosomes (13). Supporting this work, we previously found that levels of Rab11 were significantly decreased and endocytic recycling was impaired in a cell and mouse model of HD—further connecting alterations in the Rab11 function with impaired vesicle formation (15). SV size may also be altered by aberrant gain-of-function interactions of mutant htt with proteins such as the SV chaperone CSP and PACSIN1, which regulates vesicle recovery (37). Wild-type htt function is required for clathrin-mediated endocytosis during SV recovery (7), and so it is clear that several factors may contribute to this neuronal process in HD pathology. Indeed, presynaptic endocytotic dysregulation involving htt-interacting protein 1 (HIP1), an accessory protein for clathrin-mediated endocytosis, has been implicated in HD (38). This clathrin-dependent pathway of endocytosis might be relevant in explaining our findings of compromised synaptic transmission as clathrin-mediated SV recycling at *Drosophila* NMJs is fundamental for the maintenance of synaptic transmission (Fig. 5) (39). Taken together, our data point towards the mutant htt-mediated dysregulation of endocytotic

pathways leading to a reduction in SV size, with Rab11 providing a mechanism to overcome these detrimental effects. The mechanism by which Rab11 restores SV size is unclear. Previous work has indicated that wild-type htt functions in a protein complex which acts as a guanine exchange factor for Rab11 (40). Mutant htt may thus block the activation of Rab11 to its GTP-bound form by the inhibition of normal htt function in this process (13), leading to defective vesicle formation. Thus, it is possible that the overexpression of Rab11 in our system circumvents this block in activation, restoring SV size and rescuing the consequent electrophysiological and locomotor deficits.

Interestingly, two previous studies have found that the expression of a mutant htt exon 1 fragment at the murine NMJ (41) or full-length htt (Htt128Q^{FL}) at the NMJ in *Drosophila* larvae (19) enhances neurotransmission, seemingly contradicting our findings. However, the Htt128Q^{FL}-induced enhancement of release probability at the *Drosophila* larvae NMJ in this other study was observed under low, non-physiological extracellular Ca^{2+} levels (0.25 and 0.6 mm), which limits the ability to extrapolate these results to physiological conditions. Furthermore, alterations in cytosolic Ca^{2+} levels have also been implicated in the pathology of HD model mice, with reduced Ca^{2+} influx affecting neurotransmitter release (42). For these reasons, we focused our studies on observations at physiological Ca^{2+} (1.5 mm) influx levels. It is important to underscore that we observed reduced neurotransmission at the NMJ with both an htt exon 1 fragment and a full-length htt construct, suggesting a general phenomenon due to mutant htt expression. Furthermore, as Rab11 overexpression both reverses this phenotype and reduced SV size, our data are best explained by a mutant htt-mediated reduction in quantal sizes due to a decreased SV size, without changes to transmitter release probability.

We also observed the appearance of vacuoles, multivesicular bodies and multilammelar bodies in HD fly larvae, indicating increased lysosomal/autophagic activity in these cells and the diversion of membrane material into degradative organelles. However, while Rab11 overexpression significantly increased SV size and restored the electrophysiological properties of the synapse, it had no effect on the appearance of vacuoles, multivesicular bodies and multilammelar bodies. Furthermore, we did not observe any change in the number of synaptic active zones in these animals. Taken together, these data suggest that impairment in SV recycling could represent an early stage in the pathology of HD which precedes synaptic loss.

Our previous work found that the loss of dendritic spines in hippocampal neurons is correlated with proximity of the spines to mutant htt aggregates (15) and that Rab11 restores dendritic spine density—suggesting that the aggregation

Figure 3. Rab11 expression rescues the mutant htt-induced reduction in evoked transmission and quantal size. (**A**) eEJP recordings from larvae expressing Htt93Q, Htt93Q plus Rab11 or Rab11 alone. (**B**) Mean eEJP amplitudes are rescued by Rab11 expression. (**C**) Mean resting membrane potentials are similar between all genotypes. (**D**) Top, mEJP sample trace. Middle, relative cumulative frequency histogram for mEJP amplitudes: Rab11 expression (green, Htt93Q/Rab11) rescues the htt-induced reduction (grey, Htt93Q as in Figure 1D) in mEJP amplitudes. Bottom, mEJP amplitude histogram shows the right shift of amplitude distribution following Rab11 expression. (**E**) Top, mEJP sample trace. Middle, relative cumulative histogram for mEJP decay: there is no difference in decay distributions between genotypes. Bottom, mEJP decay histogram. UAS control larvae carry both the *UASHtt93Q* and the *UASRab11* insertions (genotype *w; UASRab11/+; UASHtt93Q/+*). (**F**) Summary graphs for mEJP amplitudes (i), frequencies (ii), decay (iii) and quantal content (iv). Data denote the mean ± SEM with *n* number of larvae indicated within each bar. ANOVA with *post hoc* tests. *$P < 0.05$.
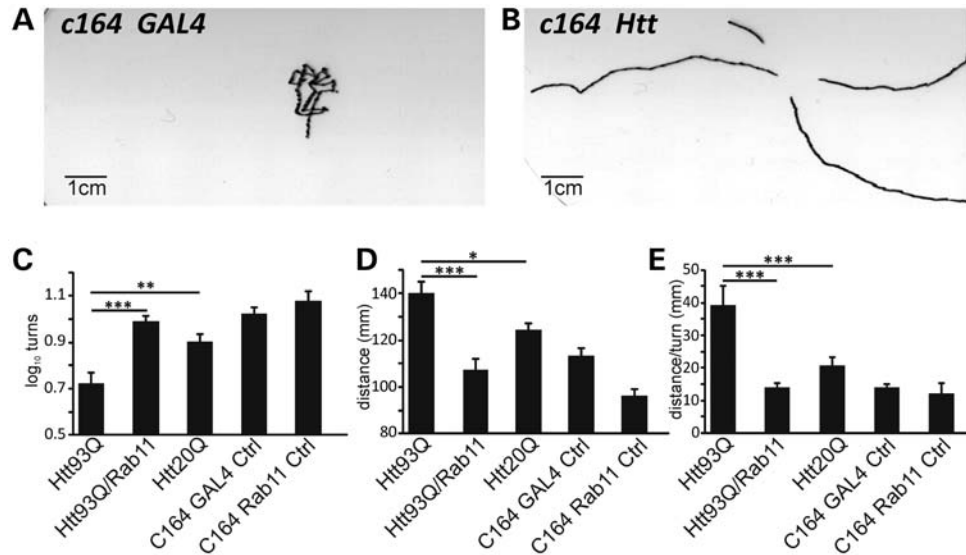
Figure 4. Defective larval crawling behaviour is rescued by Rab11. (**A**) Representative example of crawling traces produced by control larva (*w; c164GAL4/+, +*). (**B**) Trace of larva overexpressing Htt93Q in motor neurons with the *c164* driver (*w; c164GAL4/+; UASHtt93Q/+*). (**C**) Mean turns, (**D**) distance and (**E**) distance/turns in larvae overexpressing Htt93Q, Htt93Q/Rab11, Htt20Q or Gal4 and Rab11 controls driven in motor neurons by the *c164* promoter. Data are mean $\pm$ SEM. ANOVA with *post hoc* tests. $*P < 0.05$, $**P < 0.01$ and $***P < 0.001$.
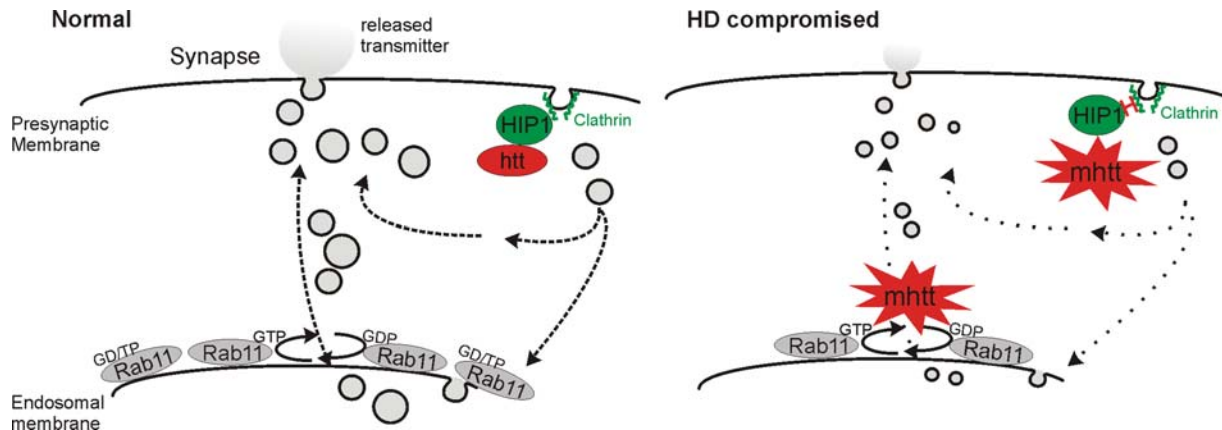

Figure 5. Model of impaired neurotransmission caused by mutant htt. Mutant htt leads to reduced SV size via reduced Rab11 function and altered interactions with HIP1, causing reduced neurotransmitter release, and synaptic dysfunction. Overexpression of Rab11 reverses these defects.

state of mutant htt could be central to synaptic phenotypes. In the current study, we find that the expression of either an exon 1 fragment (Htt93Q) or full-length mutant htt construct (Htt128^{FL}) causes a reduction in quantal size in the NMJ of *Drosophila* larvae. While third instar larvae expressing Htt93Q exhibit mutant htt containing aggregates (43), Htt128^{FL} larvae do not form mutant htt aggregates (19), suggesting that the observed synaptic dysfunction is independent of insoluble aggregates or visible inclusions. These data do not exclude the possibility that soluble oligomers of mutant htt— thought to be an important determinant in the cellular toxicity observed in HD (44)—are responsible for the observed effects on dendritic spines. Recent work in mammalian cells has found that mutant htt forms an invariant pool of oligomers that is independent of insoluble aggregate load (45), suggesting that localized differences in oligomer concentration

within a cell may be critical. Indeed, mutant htt oligomers are enriched proximal to insoluble fibrils in both mammalian cells and HD patient samples (46); thus, dendritic spines close to aggregates may be subjected to higher concentrations of oligomers. Interestingly, mutant htt also appears to block axonal transport in neurons of *Drosophila* larvae, which may play an early role in synaptic dysfunction (43,47,48). Discerning the mechanism(s) by which mutant htt alters synaptic phenotypes will be a critical area for future investigations.

Our work sheds light on the importance of Rab11 in early synaptic dysfunction in HD. These findings resonate with recent studies in HD (12–15,40) and may also impact on research in other neurodegenerative disorders, such as Alzheimer's disease and Parkinson's disease. Indeed, Rab11 activity has been found to modulate the recycling of extracellular α-synuclein (49), interact specifically with presenilin 1

(50) and play a role in oestrogen-regulated trafficking of β-amyloid in the late secretory pathway (51). It is clear that future mechanistic studies should continue to explore the role of Rab11 activity in HD pathology, and that these findings should be exploited for potential therapeutic strategies which increase Rab11 activity (52).

MATERIALS AND METHODS

Fly stocks

Flies were raised on maize media, in LD12:12 at 25°C. The *elav-GAL4* [*c155*] driver and the *w; UASRab11-GFP; +* (8506) stocks were obtained from the Bloomington Stock Center (Indiana). The *c164-GAL4* driver (36) and the full-length Htt128Q *yw; UASFLHtt128Q; +* (*M36E2*) were kindly donated by Juan Botas (Baylor College of Medicine). The *w; +; UASHttQ93 exon1* and *w; UASHtt20Q exon1* flies were a gift from J. Lawrence Marsh and Leslie Thompson (University of California, Irvine).

Electrophysiology

eEJP and mEJP were recorded with sharp electrodes from muscle 6 (abdominal segments A2/A3, Fig. 1A) of wandering third instar larvae in the current-clamp mode (MultiClamp 700B) in haemolymph-like (HL-3) solution containing 1.5 or 0.6 mM Ca^{2+} (indicated) as described previously (21). Recording electrodes (10–20 MΩ) were filled with 3 M KCl. mEJP recordings were performed in the presence of 1 μM tetrodotoxin. All eEJP/mEJPs were recorded from muscles with resting potentials more negative than −60 mV at 22°C as differences in recording temperature cause changes in glutamate receptor kinetics and amplitudes (53). All larval rearing temperatures were 25°C as temperature fluctuations result in changes of NMJ morphology and evoked responses (54). mEJPs and eEJPs were low-pass filtered at 1 kHz and digitized using a Digidata1321A. Data were collected from averaged 50 eEJPs and 120 s of mEJP recordings per muscle using pClamp 9.2 software.

Electron microscopy

Third instar larvae were 'filleted' and fixed in freshly prepared cacodylate/paraformaldehyde for 20 min at room temperature. Samples were then fixed in 2% glutaraldehyde in 0.1 M sodium cacodylate buffer (pH 7.4) at 4°C overnight and post-fixed with 1% osmium tetroxide/1% potassium ferrocyanide for 1 h at room temperature. After fixation, cells were stained *en bloc* with 5% aqueous uranyl acetate overnight at room temperature, dehydrated and embedded in Taab epoxy resin (Taab Laboratories Equipment Ltd, Aldermaston, UK). Semi-thick sections were collected onto glass slides and stained with Toluidine blue to identify areas that contained synaptic regions. Thin sections, of ∼90 nm thickness, were cut from each sample using a Reichert Ultracut S or EMU C7 ultramicrotome, collected on copper mesh grids and counter stained with 2% uranyl acetate and Reynold's lead citrate. Sections were observed using a JEOL 1220 or JEOL 1400 transmission electron microscope, using an accelerating voltage of 80 kV. Digital images were recorded using a SIS Megaview III Digital Camera with iTEM Software. SV measurements were made using ImageJ software (http://rsbweb.nih.gov/ij/index.html). A total of ∼600 SVs were measured in 11–14 boutons from three animals per genotype.

Larval crawling assay

Prior to commencing crawling assays, *Drosophila* third instar larvae were staged by propagating on maize food dyed with 0.05% Bromophenol blue, as described previously (55). As the larvae wandered, they stopped feeding and the blue dye gradually cleared from their intestines (56). Three types of wandering larvae could therefore be distinguished: those with dark blue guts (the youngest that will pupariate in 12–24 h), those with light blue guts (intermediate, will pupariate in 5–12 h) and those with an almost completely clear gut (the oldest that will pupariate in 1–6 h). Only younger, deep blue coloured, third instar larvae were used for our crawling assays. Each larva was briefly washed in distilled water and then placed in the middle of a 145-mm plate coated with 0.8% agarose. The larva was allowed to crawl for 2 min and the distance covered by it was manually drawn on transparent paper placed on the lid of the plate. The number of turns performed by each larva was counted manually. The distance crawled by each larva was calculated by scanning each larval trace and measuring its track length with Image J software (http://rsbweb.nih.gov/ij/). For each genotype, the crawling behaviour of 25–50 larvae was analysed.

The motoneuronal genotypes assayed were *c164Htt93Q* (*w/w; c164GAL4/+; UASHtt93Q/+*), *c164Htt93QRab11* (*w/w; c164GAL4/UASRab11; UASHtt93Q/+*), *c164Htt20Q* (*w/w; c164GAL4/+; UASHtt20Q/+*), *c164GAL4* (*w/w; c164GAL4/+; +/+*) and *c164Rab11* (*w/w; c164GAL4/UASRab11/+; +/+*). The number of turns was calculated by adding 1 to the actual number of turns performed by the larva, and then calculating the $\log_{10}$ of such number [$\log_{10}(n + 1)$]. This log transformation was performed to obtain a normalized distribution of the data.

Statistics

Data are expressed as mean ± SEM, where n indicates the number of muscles/larvae examined. Statistical analyses were carried out using ANOVA where applicable with the Duncan and Newman–Keuls *a posteriori* tests. Cumulative frequency distributions were compared using the K-S test. For the behavioural assays, statistical analyses were performed using ANOVA with *post hoc* tests.

SUPPLEMENTARY MATERIAL

Supplementary Material is available at *HMG* online.

ACKNOWLEDGEMENTS

Conflict of Interest statement. None declared.

FUNDING

REFERENCES

1. The Huntington's Disease Collaborative Research Group (1993) A novel gene containing a trinucleotide repeat that is expanded and unstable on Huntington's disease chromosomes. *Cell*, **72**, 971–983.
2. Gutekunst, C.A., Norflus, F. and Hersch, S.M. (2002) In: Bates, G., Harper, P.S. and Jones, L. (eds), *Huntington's Disease*. Oxford University Press, Oxford, pp. 251–275.
3. Ross, C.A. and Tabrizi, S.J. (2011) Huntington's disease: from molecular pathogenesis to clinical treatment. *Lancet Neurol.*, **10**, 83–98.
4. Paulsen, J.S., Langbehn, D.R., Stout, J.C., Aylward, E., Ross, C.A., Nance, M., Guttman, M., Johnson, S., MacDonald, M., Beglinger, L.J. *et al.* (2008) Detection of Huntington's disease decades before diagnosis: the Predict-HD study. *J. Neurol. Neurosurg. Psychiatry*, **79**, 874–880.
5. Orth, M., Schippling, S., Schneider, S.A., Bhatia, K.P., Talelli, P., Tabrizi, S.J. and Rothwell, J.C. (2010) Abnormal motor cortex plasticity in premanifest and very early manifest Huntington disease. *J. Neurol. Neurosurg. Psychiatry*, **81**, 267–270.
6. Schippling, S., Schneider, S.A., Bhatia, K.P., Munchau, A., Rothwell, J.C., Tabrizi, S.J. and Orth, M. (2009) Abnormal motor cortex excitability in preclinical and very early Huntington's disease. *Biol. Psychiatry*, **65**, 959–965.
7. Milnerwood, A.J. and Raymond, L.A. (2010) Early synaptic pathophysiology in neurodegeneration: insights from Huntington's disease. *Trends Neurosci.*, **33**, 513–523.
8. Moreno, J.A. and Mallucci, G.R. (2010) Dysfunction and recovery of synapses in prion disease: implications for neurodegeneration. *Biochem. Soc. Trans.*, **38**, 482–487.
9. Simons, K. and Zerial, M. (1993) Rab proteins and the road maps for intracellular transport. *Neuron*, **11**, 789–799.
10. Ullrich, O., Reinsch, S., Urbe, S., Zerial, M. and Parton, R.G. (1996) Rab11 regulates recycling through the pericentriolar recycling endosome. *J. Cell Biol.*, **135**, 913–924.
11. Hales, C.M., Vaerman, J.P. and Goldenring, J.R. (2002) Rab11 family interacting protein 2 associates with Myosin Vb and regulates plasma membrane recycling. *J. Biol. Chem.*, **277**, 50415–50421.
12. Li, X., Sapp, E., Chase, K., Comer-Tierney, L.A., Masso, N., Alexander, J., Reeves, P., Kegel, K.B., Valencia, A., Esteves, M. *et al.* (2009) Disruption of Rab11 activity in a knock-in mouse model of Huntington's disease. *Neurobiol. Dis.*, **36**, 374–383.
13. Li, X., Standley, C., Sapp, E., Valencia, A., Qin, Z.H., Kegel, K.B., Yoder, J., Comer-Tierney, L.A., Esteves, M., Chase, K. *et al.* (2009) Mutant huntingtin impairs vesicle formation from recycling endosomes by interfering with Rab11 activity. *Mol. Cell Biol.*, **29**, 6106–6116.
14. Li, X., Valencia, A., Sapp, E., Masso, N., Alexander, J., Reeves, P., Kegel, K.B., Aronin, N. and Difiglia, M. (2010) Aberrant Rab11-dependent trafficking of the neuronal glutamate transporter EAAC1 causes oxidative stress and cell death in Huntington's disease. *J. Neurosci.*, **30**, 4552–4561.
15. Richards, P., Didszun, C., Campesan, S., Simpson, A., Horley, B., Young, K.W., Glynn, P., Cain, K., Kyriacou, C.P., Giorgini, F. *et al.* (2011) Dendritic spine loss and neurodegeneration is rescued by Rab11 in models of Huntington's disease. *Cell Death Differ.*, **18**, 191–200.
16. Rohrbough, J. and Broadie, K. (2005) Lipid regulation of the synaptic vesicle cycle. *Nat. Rev. Neurosci.*, **6**, 139–150.
17. Marsh, J.L., Pallos, J. and Thompson, L.M. (2003) Fly models of Huntington's disease. *Hum. Mol. Genet.*, **12** (Spec No 2), R187–R193.
18. Steffan, J.S., Bodai, L., Pallos, J., Poelman, M., McCampbell, A., Apostol, B.L., Kazantsev, A., Schmidt, E., Zhu, Y.Z., Greenwald, M. *et al.* (2001) Histone deacetylase inhibitors arrest polyglutamine-dependent neurodegeneration in *Drosophila. Nature*, **413**, 739–743.
19. Romero, E., Cha, G.H., Verstreken, P., Ly, C.V., Hughes, R.E., Bellen, H.J. and Botas, J. (2008) Suppression of neurodegeneration and increased neurotransmission caused by expanded full-length huntingtin accumulating in the cytoplasm. *Neuron*, **57**, 27–40.
20. Karunanithi, S., Marin, L., Wong, K. and Atwood, H.L. (2002) Quantal size and variation determined by vesicle size in normal and mutant *Drosophila* glutamatergic synapses. *J. Neurosci.*, **22**, 10267–10276.
21. Steinert, J.R., Kuromi, H., Hellwig, A., Knirr, M., Wyatt, A.W., Kidokoro, Y. and Schuster, C.M. (2006) Experience-dependent formation and recruitment of large vesicles from reserve pool. *Neuron*, **50**, 723–733.
22. Atwood, H.L. and Karunanithi, S. (2002) Diversification of synaptic strength: presynaptic elements. *Nat. Rev. Neurosci.*, **3**, 497–516.
23. Katz, B. and Miledi, R. (1967) A study of synaptic transmission in the absence of nerve impulses. *J. Physiol.*, **192**, 407–436.
24. DiAntonio, A., Petersen, S.A., Heckmann, M. and Goodman, C.S. (1999) Glutamate receptor expression regulates quantal size and quantal content at the *Drosophila* neuromuscular junction. *J. Neurosci.*, **19**, 3023–3032.
25. Marrus, S.B., Portman, S.L., Allen, M.J., Moffat, K.G. and DiAntonio, A. (2004) Differential localization of glutamate receptor subunits at the *Drosophila* neuromuscular junction. *J. Neurosci.*, **24**, 1406–1415.
26. Petersen, S.A., Fetter, R.D., Noordermeer, J.N., Goodman, C.S. and DiAntonio, A. (1997) Genetic analysis of glutamate receptors in *Drosophila* reveals a retrograde signal regulating presynaptic transmitter release. *Neuron*, **19**, 1237–1248.
27. Daniels, R.W., Collins, C.A., Gelfand, M.V., Dant, J., Brooks, E.S., Krantz, D.E. and DiAntonio, A. (2004) Increased expression of the *Drosophila* vesicular glutamate transporter leads to excess glutamate release and a compensatory decrease in quantal content. *J. Neurosci.*, **24**, 10466–10474.
28. Czaja, M.J. (2010) Autophagy in health and disease. 2. Regulation of lipid metabolism and storage by autophagy: pathophysiological implications. *Am. J. Physiol. Cell Physiol.*, **298**, C973–C978.
29. Renger, J.J., Ueda, A., Atwood, H.L., Govind, C.K. and Wu, C.F. (2000) Role of cAMP cascade in synaptic stability and plasticity: ultrastructural and physiological analyses of individual synaptic boutons in *Drosophila* memory mutants. *J. Neurosci.*, **20**, 3980–3992.
30. Davis, G.W., DiAntonio, A., Petersen, S.A. and Goodman, C.S. (1998) Postsynaptic PKA controls quantal size and reveals a retrograde signal that regulates presynaptic transmitter release in *Drosophila. Neuron*, **20**, 305–315.
31. Wang, J.W., Sylwester, A.W., Reed, D., Wu, D.A., Soll, D.R. and Wu, C.F. (1997) Morphometric description of the wandering behavior in *Drosophila* larvae: aberrant locomotion in Na+ and K+ channel mutants revealed by computer-assisted motion analysis. *J. Neurogenet.*, **11**, 231–254.
32. Wang, J.W., Soll, D.R. and Wu, C.F. (2002) Morphometric description of the wandering behavior in *Drosophila* larvae: a phenotypic analysis of K+ channel mutants. *J. Neurogenet.*, **16**, 45–63.
33. Cheng, L.E., Song, W., Looger, L.L., Jan, L.Y. and Jan, Y.N. (2010) The role of the TRP channel NompC in *Drosophila* larval and adult locomotion. *Neuron*, **67**, 373–380.
34. Nishimura, Y., Yalgin, C., Akimoto, S., Doumanis, J., Sasajima, R., Nukina, N., Miyakawa, H., Moore, A.W. and Morimoto, T. (2010) Selection of behaviors and segmental coordination during larval locomotion is disrupted by nuclear polyglutamine inclusions in a new *Drosophila* Huntington's disease-like model. *J. Neurogenet.*, **24**, 194–206.
35. Lanson, N.A. Jr, Maltare, A., King, H., Smith, R., Kim, J.H., Taylor, J.P., Lloyd, T.E. and Pandey, U.B. (2011) A *Drosophila* model of FUS-related neurodegeneration reveals genetic interaction between FUS and TDP-43. *Hum. Mol. Genet.*, **20**, 2510–2523.
36. Pennetta, G., Hiesinger, P.R., Fabian-Fine, R., Meinertzhagen, I.A. and Bellen, H.J. (2002) *Drosophila* VAP-33A directs bouton formation at neuromuscular junctions in a dosage-dependent manner. *Neuron*, **35**, 291–306.
37. Smith, R., Brundin, P. and Li, J.Y. (2005) Synaptic dysfunction in Huntington's disease: a new perspective. *Cell Mol. Life Sci.*, **62**, 1901–1912.
38. Parker, J.A., Metzler, M., Georgiou, J., Mage, M., Roder, J.C., Rose, A.M., Hayden, M.R. and Neri, C. (2007) Huntingtin-interacting protein 1 influences worm and mouse presynaptic function and protects

Caenorhabditis elegans neurons against mutant polyglutamine toxicity. *J. Neurosci.*, **27**, 11056–11064.

39. Verstreken, P., Ohyama, T. and Bellen, H.J. (2008) FM 1–43 labeling of synaptic vesicle pools at the *Drosophila* neuromuscular junction. *Methods Mol. Biol.*, **440**, 349–369.

40. Li, X., Sapp, E., Valencia, A., Kegel, K.B., Qin, Z.H., Alexander, J., Masso, N., Reeves, P., Ritch, J.J., Zeitlin, S. *et al.* (2008) A function of huntingtin in guanine nucleotide exchange on Rab11. *Neuroreport*, **19**, 1643–1647.

41. Rozas, J.L., Gomez-Sanchez, L., Tomas-Zapico, C., Lucas, J.J. and Fernandez-Chacon, R. (2011) Increased neurotransmitter release at the neuromuscular junction in a mouse model of polyglutamine disease. *J. Neurosci.*, **31**, 1106–1113.

42. Hodgson, J.G., Agopyan, N., Gutekunst, C.A., Leavitt, B.R., LePiane, F., Singaraja, R., Smith, D.J., Bissada, N., McCutcheon, K., Nasir, J. *et al.* (1999) A YAC mouse model for Huntington's disease with full-length mutant huntingtin, cytoplasmic toxicity, and selective striatal neurodegeneration. *Neuron*, **23**, 181–192.

43. Sinadinos, C., Burbidge-King, T., Soh, D., Thompson, L.M., Marsh, J.L., Wyttenbach, A. and Mudher, A.K. (2009) Live axonal transport disruption by mutant huntingtin fragments in *Drosophila* motor neuron axons. *Neurobiol. Dis.*, **34**, 389–395.

44. Truant, R., Atwal, R.S., Desmond, C., Munsie, L. and Tran, T. (2008) Huntington's disease: revisiting the aggregation hypothesis in polyglutamine neurodegenerative diseases. *FEBS J.*, **275**, 4252–4262.

45. Olshina, M.A., Angley, L.M., Ramdzan, Y.M., Tang, J., Bailey, M.F., Hill, A.F. and Hatters, D.M. (2010) Tracking mutant huntingtin aggregation kinetics in cells reveals three major populations that include an invariant oligomer pool. *J. Biol. Chem.*, **285**, 21807–21816.

46. Legleiter, J., Mitchell, E., Lotz, G.P., Sapp, E., Ng, C., DiFiglia, M., Thompson, L.M. and Muchowski, P.J. (2010) Mutant huntingtin fragments form oligomers in a polyglutamine length-dependent manner in vitro and in vivo. *J. Biol. Chem.*, **285**, 14777–14790.

47. Gunawardena, S., Her, L.S., Brusch, R.G., Laymon, R.A., Niesman, I.R., Gordesky-Gold, B., Sintasath, L., Bonini, N.M. and Goldstein, L.S. (2003) Disruption of axonal transport by loss of huntingtin or expression of pathogenic polyQ proteins in *Drosophila*. *Neuron*, **40**, 25–40.

48. Lee, W.C., Yoshihara, M. and Littleton, J.T. (2004) Cytoplasmic aggregates trap polyglutamine-containing proteins and block axonal transport in a *Drosophila* model of Huntington's disease. *Proc. Natl Acad. Sci. USA*, **101**, 3224–3229.

49. Liu, J., Zhang, J.P., Shi, M., Quinn, T., Bradner, J., Beyer, R., Chen, S. and Zhang, J. (2009) Rab11a and HSP90 regulate recycling of extracellular alpha-synuclein. *J. Neurosci.*, **29**, 1480–1485.

50. Dumanchin, C., Czech, C., Campion, D., Cuif, M.H., Poyot, T., Martin, C., Charbonnier, F., Goud, B., Pradier, L. and Frebourg, T. (1999) Presenilins interact with Rab11, a small GTPase involved in the regulation of vesicular transport. *Hum. Mol. Genet.*, **8**, 1263–1269.

51. Greenfield, J.P., Leung, L.W., Cai, D., Kaasik, K., Gross, R.S., Rodriguez-Boulan, E., Greengard, P. and Xu, H. (2002) Estrogen lowers Alzheimer beta-amyloid generation by stimulating trans-Golgi network vesicle biogenesis. *J. Biol. Chem.*, **277**, 12128–12136.

52. Agola, J., Jim, P., Ward, H., Basuray, S. and Wandinger-Ness, A. (2011) Rab GTPases as regulators of endocytosis, targets of disease and therapeutic opportunities. *Clin. Genet.*, **80**, 305–318.

53. Postlethwaite, M., Hennig, M.H., Steinert, J.R., Graham, B.P. and Forsythe, I.D. (2007) Acceleration of AMPA receptor kinetics underlies temperature-dependent changes in synaptic strength at the rat calyx of Held. *J. Physiol.*, **579**, 69–84.

54. Sigrist, S.J., Reiff, D.F., Thiel, P.R., Steinert, J.R. and Schuster, C.M. (2003) Experience-dependent strengthening of *Drosophila* neuromuscular junctions. *J. Neurosci.*, **23**, 6546–6556.

55. Andres, A.J. and Thummel, C.S. (1994) Methods for quantitative analysis of transcription in larvae and prepupae. *Methods Cell Biol.*, **44**, 565–573.

56. Maroni, G. and Laurie-Ahlberg, C.C. (1983) Genetic control of Adh expression in *Drosophila melanogaster*. *Genetics*, **105**, 921–933.